Numerical Simulation of Dehydrogenation of Liquid Steel in the Vacuum Tank Degasser

SHAN YU and SEPPO LOUHENKILPI

Vacuum tank degassers are often utilized to remove hydrogen from liquid steel. A new comprehensive numerical model, which has been developed to simulate hydrogen removal in the vacuum degassers, is presented in this paper. The degassing model consists of two sub-models, which calculate the gas-steel flow field and the species transport of hydrogen. An extended k–ε turbulence model is adopted to consider the effect of gas injection on the turbulent properties and an interfacial area concentration model is introduced to compute the interfacial area density between liquid steel and the bubbles. The fluid dynamic sub-model is validated with a physical gas stirred tank, which is believed to have similar flow phenomena as the studied vacuum degasser based on the modified Froude number. Two fundamental expressions for mass transfer coefficient, which have been paid little attention by the researchers concentrating on vacuum degassing, are evaluated with a simulation case corresponding to practical operation. The effect of vacuum pressure on the dehydrogenation process is investigated and, moreover, the integrated model is verified with industrial measurements. The predicted final hydrogen contents in liquid steel show good agreement with the measured ones. The model and the main results are presented.

I. INTRODUCTION

IT is well known that in the production of special steels, the control of hydrogen in steel is of special importance since hydrogen can lead to many problems such as the formation of flakes, the occurrence of breakouts, and hydrogen embrittlement. The content of hydrogen in liquid steel can sometimes be required to be 1 ppm or lower and if the level of hydrogen in solid steel after casting is still too high, additional heat treatment in the hydrogen removal furnace is needed, which can take several days.

The hydrogen pickup and removal in liquid steel are both complicated and the net hydrogen level in steel depends on the extent of pickup and removal during various stages of the steelmaking process. Hydrogen sources are refractory materials, lime, alloying elements, scrap, atmosphere, *etc*. Moisture from additions for deoxidation and alloying have also been found to increase the hydrogen content in liquid steel.[1] Because the solubility of hydrogen in liquid steel is considerably higher than in solid steel, it is a prerequisite to remove hydrogen from liquid steel before casting. In steelmaking industries, the removal of hydrogen in liquid steel is usually accomplished within the vacuum tank degasser in which intensive gas stirring and vacuum treatment are utilized to provide favorable conditions for dehydrogenation. The main parameters that influence the hydrogen removal in the tank degasser are vacuum pressure, treatment time, liquid steel composition, flow rates of stirring gas, and circulation flow in the liquid bath. It has been reported that the efficient removal can be obtained at the bath surface and areas close to the gas plume, where hydrogen can be picked up by the argon bubbles.[2]

In general, the vacuum degassing equipment will probably not change drastically and it is impossible to observe the degassers and take steel samples under vacuum and high temperature. Therefore, the main phenomena in the vacuum degasser, such as fluid flow and mass transfer, have been studied experimentally and numerically for decades.[3–10] Compared to physical modeling, the numerical approach has been receiving more attention nowadays mostly due to its incomparable advantages: The numerical approach only has a little difficulty in representing the processes with high temperature and large scale dimensions. In addition, there is no inaccessible location in a computational domain and no disturbance caused by a probe, which commonly occur in a physical model.[11] In principle, the multiphase flow (*e.g.*, gas–liquid flow in the vacuum degasser) can be modeled with the Euler–Euler (two-fluid) method or by using the Lagrangian particle tracking technique. The former one treats each phase as an interpenetrating continuum. In contrast, the latter one treats a dispersed phase as a large number of particles, bubbles, or droplets. The point to be noticed is that the effect of volume fraction of the dispersed phase is neglected in this technique, which is questioned if the share of the

SHAN YU, Doctoral Candidate, and SEPPO LOUHENKILPI, Professor, are with the Laboratory of Metallurgy, Department of Materials Science and Engineering, Aalto University, PO Box 16200, Vuorimiehentie 2, Espoo 00076, Aalto, Finland. Contact e-mail: shan.yu@aalto.fi

dispersed phase becomes significant in the flow. Domgin et al.[3] studied the two-phase flow in gas stirred ladle using both approaches and reported that the calculated results obtained by the two-fluid method show correct agreement with the experimental ones, especially in terms of mean velocities. However, the turbulent kinetic energy (TKE) is generally underestimated. The reason for the deviation could be related to the usage of the standard $k–\varepsilon$ model in the study. The applicability of the standard $k–\varepsilon$ model for such a gas stirred flow system was discussed by the other authors[4,5] and extra terms that consider the turbulence induced by the dispersed bubbles were suggested to extend the standard $k–\varepsilon$ equations.

The transport of dissolved hydrogen in the bath of liquid steel is usually solved, as a rule, after the flow field has been predicted.[9–13] In the vacuum degasser, the mass transfer of hydrogen in the bubble and the interfacial reaction are believed to be fast. The overall dehydrogenation rate is thus limited by the mass transfer in liquid steel, which is under strong convective condition induced by the intensive gas stirring. It is therefore necessary to know the convective mass transfer coefficient in liquid steel (hereinafter called mass transfer coefficient in brief) for solving the species equations. In practice, Higbie and Danckwerts (eddy-cell) expressions are frequently adopted to compute the mass transfer coefficient in such a system. Higbie[14] assumed that mass transfer in a gas–liquid system is related to the surface renewal time, which is a function of bubble diameter and slip velocity. An expression including these variables has been given to calculate the mass transfer coefficient. However, the expression was announced to be suitable for systems at low TKE dissipation by Alves et al.[15] On the other hand, Danckwerts proposed that the mass transfer in gas–liquid system mainly depends on the motion of small-scale eddies and thus the mass transfer coefficient could be a function of TKE dissipation. Taniguchi et al.[16] employed these two expressions to compute the concentration of CO_2 in a CO_2–water system. The results showed that the eddy-cell expression is more accurate in the bubble-dispersion region, where TKE dissipation is high. To the best of our knowledge, these two fundamental expressions of mass transfer coefficient have not been thoroughly evaluated and applied in the studies of dehydrogenation process in the vacuum degasser. This is one of the motivations behind this work.

In the present paper, a comprehensive numerical model is developed to investigate the complex flow behavior and dehydrogenation process in an industrial vacuum tank degasser. In the integrated model, equations of multiphase flow and species transport are solved and an extended turbulent model is used to consider the effect of gas bubbles. Moreover, a one-group interfacial area concentration (IAC) model is employed to obtain the distribution of IAC and the two fundamental expressions of mass transfer coefficient (Higbie and eddy-cell) are assessed with a simulation case. All simulations are performed with ANSYS FLUENT 14.0 augmented by user-defined functions (UDF).[17,18] The simulations are validated both with a physical gas stirred tank (from the literature) and with measurements from an industrial vacuum tank degassing plant. The effect of vacuum pressure on hydrogen removal and the distribution of hydrogen removal through the bubble surface and bath surface are investigated.

II. INDUSTRIAL CASE AND MODEL DESCRIPTION

An industrial vacuum degasser from Riva Caronno Works in Italy is simulated in this work. As depicted in Figure 1, the porous plug (nozzle) is located at 0.695 m from the center of the bottom. Other dimensions are also shown in the figure. The evolution of the operation pressure is illuminated in Figure 2. The pressure is lowered rapidly and then reaches a stable condition of deep vacuum (typically under 1.33 mbar), which will last for the remaining period. The argon gas with a high flow rate of 0.15 Nm^3/min is injected at the beginning (lasting about 1 minute) of the deep vacuum condition to create the open-eye. After that, the gas flow rate is reduced to 0.05 Nm^3/min, which is low compared with many other steel plants. During the entire 25-minute treatment, the temperature varies from 1913 K to 1868 K (1640 °C to 1595 °C) and the hydrogen content in liquid steel descends from 6.1 to 1.7 ppm.

In this study, a comprehensive numerical model is established to simulate the flow behavior and dehydrogenation process in the industrial vacuum degasser during the period from the moment when the open-eye is created to the treatment end (e.g., Figure 2, 18 minutes). The integrated model is divided into two sub-models: one for the (multiphase) flow pattern and the other for the hydrogen transport. Some simplifications and assumptions are applied.
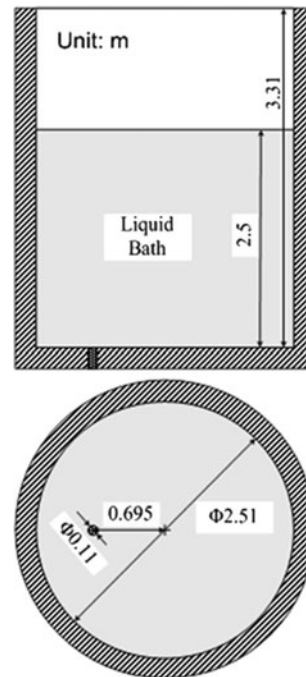

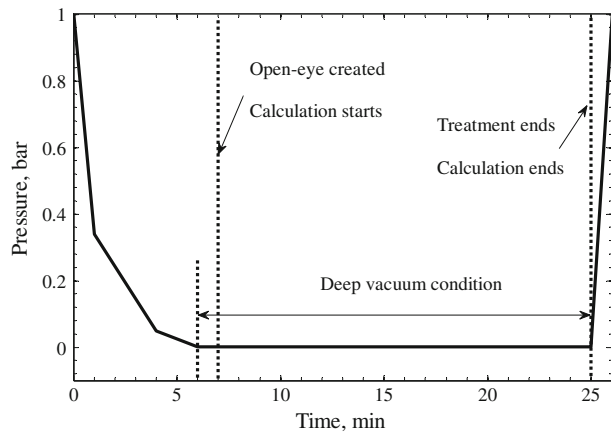Fig. 1—Schematic structure of the vacuum degasser.

Fig. 2—Evolution of the operation pressure during the treatment.

(a) The effect of temperature drop (*i.e.*, 45 K (45 °C) in the industrial degasser) is assumed to be minor and the model is isothermal. The temperature used in the model is 1873 K (1600 °C).

(b) Slag is neglected in the simulation. The lime addition in the slag phase, which is used to carry out desulfurization during degassing, often contains moisture and this would increase the hydrogen content in vacuum degassers. However, lime is added only during EAF tapping and the humidity content of the lime is about 1 pct in the current case (of Riva Caronno Works). The slag phase is therefore neglected.

(c) The bath surface in the vacuum degasser is assumed to be flat. The vacuum and zero-H_2 atmosphere conditions are numerically imposed on the bath surface despite the condition of zero-H_2 not being exactly true in practice.

(d) The hydrogen is removed through purging bubbles and the bath surface. It is assumed that dehydrogenation at the bath surface only happens where the open-eye is located. The open-eye region at the bath surface is generated using a threshold of gas volume fraction in the top cells (adjacent to the bath surface), *i.e.*, the top cells in which the calculated gas fractions are greater than the threshold are marked within the open-eye. The threshold is adjusted by

trial and error until the size of the open-eye is about 0.45 to 0.55 m, which is based on the observations from Riva. The threshold applied in the model is 2 pct.

(e) The effect of surface active elements (*e.g.*, sulfur and oxygen) in liquid steel on dehydrogenation is not

considered. It is well known that surface active elements have a significant effect on nitrogen removal, but it is typically assumed that their effect on hydrogen removal is negligible.

(f) The decarburization process during vacuum degassing and its effect on dehydrogenation are neglected. In the simulated cases from Riva Caronno Works, the total oxygen content is very low (30 to 40 ppm) and decarburization reaction is insignificant. The decarburization product (CO) and its effect on dehydrogenation are therefore neglected.

A. *Fluid Dynamics of Multiphase Flow*

The Euler–Euler method is applied to solve the gas–liquid system in the vacuum degasser and an extended $k–\varepsilon$ model is used to include the influence of gas injection on turbulent properties. The conservation equations are presented below.

The continuity equation for phase "q" (*i.e.*, gas or liquid steel) is

$$\nabla \cdot (\alpha_q \rho_q \mathbf{u}_q) = 0 \qquad [1]$$

where α, ρ, and $\mathbf{u}$ are volume fraction, density, and velocity vector, respectively.

The momentum equation for phase "q" is

$$\nabla \cdot (\alpha_q \rho_q \mathbf{u}_q \mathbf{u}_q) = -\alpha_q \nabla P + \nabla \cdot (\alpha_q \mu_{\text{eff},q} \nabla \mathbf{u}_q) + \alpha_q \rho_q \mathbf{g} + \mathbf{F}_{pq} + \mathbf{R}_{pq} \qquad [2a]$$

where P and μ_{eff} are pressure and effective viscosity, respectively, the subscript "p" stands for the phase besides phase "q." The lift force $\mathbf{F}_{pq}$ and drag force $\mathbf{R}_{pq}$ are considered because of the interaction between gas bubbles and liquid steel and are expressed as

$$\mathbf{F}_{pq} = -C_L \alpha_p \rho_q (\mathbf{u}_p - \mathbf{u}_q) \times (\nabla \times \mathbf{u}_q) \qquad [2b]$$

$$\mathbf{R}_{pq} = C_D \frac{\alpha_q \alpha_p \rho_p \text{Re}}{24\theta} (\mathbf{u}_p - \mathbf{u}_q) \qquad [2c]$$

where C_L and θ are the lift coefficient and bubble relaxation time, respectively. The drag coefficient C_D is determined by the following expressions:

$$C_D = \begin{cases} C_{\text{vis}} = \frac{24}{\text{Re}} (1 + 0.1\text{Re}^{0.75}) & C_D < C_{\text{vis}} \\ C_{\text{dis}} = \frac{2}{3} \frac{d_b}{\lambda_{\text{RT}}} \left(\frac{1+17.67f^{6/7}}{18.67f} \right); f = (1 - \alpha_p)^{1.5} & C_{\text{vis}} < C_{\text{dis}} < C_{\text{cap}} \\ C_{\text{cap}} = \frac{8}{3} (1 - \alpha_p)^2 & C_{\text{dis}} < C_{\text{cap}} \end{cases} \qquad [2d]$$

where d_b and λ_{RT} are the bubble diameter and Rayleigh–Taylor instability wavelength, respectively. In this study, the bubble diameter, d_b, is assumed to be 0.008 m.

The standard $k–\varepsilon$ mixture model for turbulence calculation is shown as

$$\nabla \cdot (\rho_m k \mathbf{u}_m) = \nabla \cdot \left(\frac{\mu_{t,m}}{\sigma_k} \nabla k \right) + G_k - \rho_m \varepsilon + S_k \quad [3a]$$

$$\nabla \cdot (\rho_m \varepsilon \mathbf{u}_m) = \nabla \cdot \left(\frac{\mu_{t,m}}{\sigma_\varepsilon} \nabla \varepsilon \right) + \frac{\varepsilon}{k} (C_{1\varepsilon} G_k - C_{2\varepsilon} \rho_m \varepsilon) + S_\varepsilon$$

$$[3b]$$

where the subscript "m" denotes the mixture (volume-averaged) quantity and μ_t and G_k are eddy viscosity and production of TKE, respectively. S_k and S_ε are the source terms in the equations (zero by default).

The above standard equations should not be directly applied in a vacuum degasser where the bubbles could magnify turbulence in the bulk liquid as a result of interfacial interactions, such as drag, wake shedding, and bubble wobbling. In order to take such aspects into account, an extended k–ε mixture model has been proposed by setting the source terms as[5]

$$S_k = C_{k1} \alpha_g (1 - \alpha_g) G_k + C_{k2} C_f \alpha_g \rho_l k \quad [3c]$$

$$S_\varepsilon = C_{\varepsilon 1} \alpha_g (1 - \alpha_g) G_k \frac{\varepsilon}{k} + C_{\varepsilon 2} C_f \alpha_g \rho_l \varepsilon \quad [3d]$$

where the subscripts "l" and "g" stand for the liquid phase and gas phase, respectively.

B. Species Transport of Hydrogen

In principle, hydrogen is removed *via* two routes in a vacuum degasser. On the one hand, hydrogen can be taken in by the bubble with low partial pressure of hydrogen. The bubble will keep absorbing hydrogen and floating up in the liquid steel bath, and finally the hydrogen-enriched bubble will go out of the bath. On the other hand, dehydrogenation could also take place directly at the bath surface where the open-eye is located. The hydrogen dissolved in the liquid steel ([H]) transforms to hydrogen gas (H_2) following the reaction

$$2[H] = H_2 \quad [4a]$$

This reaction is controlled by the Sievert's law and the transformed expressions of the law are[19,20]

$$\frac{Y_{H,e}}{10^{-7}} = \frac{K_H}{\xi_H} \sqrt{P_{H_2}} \quad [4b]$$

$$\log K_H = -\frac{1900}{T} + 0.9201 \quad [4c]$$

where $Y_{H,e}$, K_H, P_{H_2}, and T are the equilibrium mass fraction of hydrogen in liquid steel, equilibrium constant, partial pressure of hydrogen in the bubble, and temperature [*i.e.*, 1873 K (1600 °C)], respectively. The hydrogen activity coefficient ξ_H is calculated by

$$\log \xi_H = \Sigma \psi_H^j [\text{pct } j] \quad [4d]$$

where ψ_H^j and [pct j] are the interaction coefficient and mass percent concentration of element "j" in liquid steel, respectively. The composition of liquid steel in the vacuum degasser from Riva Caronno Works is listed in Table I, where the corresponding interaction coefficients are also included.

The species transport equation, which is used to compute the transient distribution of hydrogen in phase "q," is as follows:

$$\frac{\partial}{\partial t} (\alpha_q \rho_q Y_{i,q}) + \nabla \cdot (\alpha_q \rho_q Y_{i,q} \mathbf{u}_q) = -\nabla \cdot (\alpha_q \mathbf{J}_{i,q}) + S_{i,q}$$

$$[5a]$$

where subscript "i" denotes [H] or H_2 corresponding to the solved phase and $Y_{i,q}$ and $\mathbf{J}_{i,q}$ are species mass fraction and diffusive flux in each phase, respectively. The source term $S_{i,q}$ for the different phase has the following relation as a result of mass conservation,

$$S_{[H],l} = -S_{H_2,g} \quad [5b]$$

and $S_{[H],l}$ is computed by the convective mass transfer equation,

$$S_{[H],l} = \kappa \cdot a \cdot \rho_l (Y_{H,e} - Y_H) \quad [5c]$$

where κ, a, and Y_H are the mass transfer coefficient in liquid, IAC, local hydrogen concentration in the computational cell, respectively. At the bath surface, the equilibrium hydrogen concentration $Y_{H,e}$ is 0 because of the zero-H_2 condition.

For the mass transfer coefficient, both Higbie's and eddy-cell expressions are evaluated. The Higbie's expression is written as

$$\kappa = 2 \left(\frac{D_H}{\pi \tau} \right)^{1/2} \quad [6a]$$

$$D_H = D_{mole} + \frac{v}{Sc}; \quad \tau = \begin{cases} d_b/u_{slip} & \text{for the bubble} \\ r_{open-eye}/u_r & \text{for the bath surface} \end{cases}$$

$$[6b,c]$$

where D_H, D_{mole}, v, Sc, τ, u_{slip}, u_r, and $r_{open-eye}$ are the diffusivity of hydrogen dissolved in liquid steel, molecular diffusivity(10^{-7} m^2/s for hydrogen in liquid steel), kinematic viscosity, Schmidt number ($Sc = 1$), the

Table I. Liquid Steel Composition and Interaction Coefficients[20] for Dissolved Hydrogen

Element	C	Mn	Si	P	S	Cr	Ni	Cu	Ti	B
[pct j]	0.382	1.08	0.22	0.0129	0.0174	0.203	0.0532	0.145	0.0611	0.0034
ψ_H^j	0.06	−0.001	0.027	0.011	0.008	−0.002	−0.002	0.0005	0.08	0.05

residence time of liquid, slip velocity, radial velocity at bath surface, and radius of the open-eye, respectively.

The eddy-cell expression is[16]

$$\kappa = 0.3 \left(D_H \sqrt{\frac{\varepsilon}{\nu}} \right)^{1/2} \quad [6d]$$

C. *Interfacial Area Concentration*

The one-group IAC model, which has been thoroughly described by Wu et al.[21] and Hibiki et al.,[22] is employed to calculate the IAC (cf. Eq. [5c]). The conservation equation is

$$\nabla \cdot \left(\alpha_g \rho_g a \mathbf{u}_g \right) = \alpha_g \rho_g (S_{RC} + S_{WE} + S_{TI}) - \alpha_g \rho_g a \nabla \mathbf{u}_g \quad [7]$$

where S_{RC}, S_{WE}, and S_{TI} are the terms of bubble coalescence induced by random collision, bubble coalescence induced by wake-entrainment, and bubble breakup induced by turbulent impact, respectively.

D. *Boundary Treatment*

The surface of the liquid steel bath is treated as flat and only gas can escape through the (free) surface. This is realized by adding a set of sink terms into the conservation equations of gas phase in each control volume adjacent to the surface.[7] The sink terms are given by

$$S_\phi = -\varphi \alpha_g \rho_g \max\left(w_g, 0\right) \frac{A_{fs}}{V_{cv}} \quad \varphi = 1, \mathbf{u}, k, \varepsilon, Y_i \quad [8]$$

where w_g, A_{fs}, and V_{cv} are the gas velocity perpendicular to the free surface, free surface area, and volume of numerical grid (control volume), respectively.

The non-slip condition is applied for the liquid, while the slip condition is imposed for the gas at the walls. To evaluate the IAC, the initial value for the IAC at the gas inlet is given by empirical formula[22]

$$a_0 = 1.64 \, \tilde{L}_0^{-1.127} \, \alpha_0^{0.851} \, \tilde{\varepsilon}_0^{0.0318} \quad [9]$$

where $\tilde{L}_0$ is the dimensionless Laplace length.

The pressure in the argon bubbles is simplified as

$$P_b = P_v + \sum_{ii=\text{cells above}} \left(\rho_g \alpha_{g,\,ii} + \rho_l \alpha_{l,\,ii} \right) g h_{\text{cell},\,ii} \quad [10]$$

where P_v, $|\mathbf{g}|$, and h_{cell} are vacuum pressure, gravity magnitude, and height of each cell above the bubble, respectively. The coefficients and constants in the equations of this section are listed in Table II.

III. MODEL VALIDATION AND ANALYSIS

A. *Multiphase Flow*

The multiphase flow calculation in the vacuum degasser should be firstly verified before it is adopted to solve the hydrogen transport equations. However, it is practically impossible to measure or observe the flow field in an industrial vacuum degasser. As a result, experimental water modeling, which is based on the similarity laws, has been widely employed to investigate characteristic phenomena in such gas–liquid systems.

An experimental study of gas–liquid flow in a gas stirred tank has been conducted by Sheng et al.[5,6] The comparisons of main parameters between this physical model and the vacuum degasser from Riva Caronno Works are shown in Table III, where Fr_{md} is quite close between the two systems. The developed fluid dynamic model is therefore applied to and validated with Sheng's physical model and the corresponding results.[5,6] In Table III, the size of the porous nozzle (cf. Figure 1) is converted to hydraulic diameter as a single-hole nozzle. The modified Froude numbers are expressed as

$$Fr_{md} = \frac{4Q}{\pi d_{hyc}^2} \frac{1}{\sqrt{|\mathbf{g}|H}} \sqrt{\frac{\rho_g}{\rho_l - \rho_g}} \quad [11]$$

where Q, d_{hyc}, and H are gas flow rate, nozzle hydraulic diameter, and bath height, respectively.

Figure 3 shows the comparison between the measured and calculated liquid velocity fields. In general, the circulating flow, which is located at the upper part of the bath, occurs as a main feature in both domains. The liquid flows upward in the central region because of the gas injection. The flow direction tilts gradually and is directed to the ladle sidewall near the bath surface and, finally, the liquid flows downward along the sidewall when it is far from the intensive injection zone.

The comparisons of measured and calculated axial velocity and TKE along the center line are illustrated in Figures 4 and 5, respectively. The calculated results by the standard k–ε model (no extra terms) are also shown in the figures. As can be seen, the accuracy of prediction can be improved by adding extra terms into the turbulent equations, i.e., extended turbulent model. In

Table II. Coefficients and Constants in the Equations

C_L	$C_{1\varepsilon}$	$C_{2\varepsilon}$	σ_k	σ_ε	C_{k1}	C_{k2}	$C_{\varepsilon1}$	$C_{\varepsilon2}$
0.1	1.44	1.92	1.0	1.3	6.0	0.75	4.0	0.6

Table III. Comparisons of the Main Parameters Between the Riva Ladle and the Physical Water Model

	Riva Ladle	Physical Water Model[5,6]
Vessel diameter (m)	2.51	0.5
Nozzle hydraulic diameter (mm)	5.7	4.0
Bath height (m)	2.5	0.42
Liquid density (kg/m³)	7100	998
Liquid viscosity (Pa s)	0.005	0.001
Gas density (kg/m³)	0.48*	1.225
Gas viscosity (Pa s) × 10^5	8.4*	1.79
Gas flow rate (m³/s) × 10^3	3.0*	0.05 to 0.15
Fr_{md} (–)	0.20	0.068 to 0.21

*Properties of argon at temperature of 1873 K (1600 °C), pressure of 1.7×10^5 Pa.
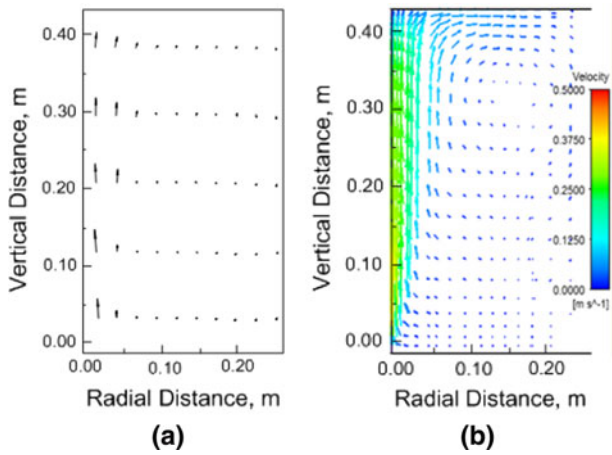
Fig. 3—Comparison of the velocity field between the water model by Sheng *et al.*[5,6] and simulation ($Q = 5.0 \times 10^{-5}$ Nm³/s): (*a*) measured and (*b*) calculated.

general, the computational results using the extended turbulent model show correct trends compared with the experimental data.[5,6] However, the deviations of axial liquid velocity and TKE become greater near the boundaries, *e.g.*, vessel bottom and bath surface. This calls for a more advanced turbulent model because the k–ε equations are known to overpredict the turbulence especially in strongly curved flows, which usually happen at the boundaries. Nevertheless, the developed fluid dynamic multiphase model presented in Section II seems to be accurate enough to investigate the complex flow behavior in the industrial vacuum degasser.

B. Mass Transfer Coefficient of Hydrogen in Liquid Steel

As mentioned above, there are two main expressions (Higbie's and eddy-cell) to compute the mass transfer coefficient of hydrogen in liquid steel, which is crucial for the species transport equations. The two expressions are evaluated with simulations using practical dimensions and typical operation conditions from Riva Caronno Works, as shown in Figure 2. The vacuum pressure is 1 mbar, the initial hydrogen content in liquid steel (hereinafter denoted as [H]) is 6.1 ppm, and the gas flow rate (Q) is 0.05 Nm³/min.

The evolutions of hydrogen removal ratio and the [H] are depicted in Figure 6, where the measured final [H] and hydrogen removal ratio from the plant (data) are also plotted. It can be seen that the curves with both expressions have very similar trends: The [H] descends during the treatment and its removal ratio rises. However, the results with eddy-cell expression give better agreement with the measured data (*cf*. Figure 6). This claim should be supported with more practical data collected during the vacuum degassing process, which unfortunately are difficult to obtain. The applicability of each expression, *i.e.*, Higbie's or eddy-cell, has been discussed by Alves *et al.*,[15] who pointed out that Higbie's expression could be more suitable for the system with a low level of TKE dissipation because bubble size is much higher than the eddy scale when
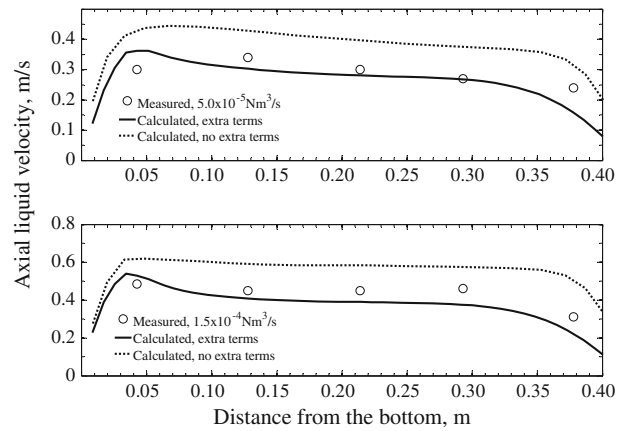

Fig. 4—Comparisons between measured[5,6] and calculated axial liquid velocity along the center line with gas flow rate $Q = 5.0 \times 10^{-5}$ Nm³/s (upper panel) and $Q = 1.5 \times 10^{-4}$ Nm³/s (lower panel).
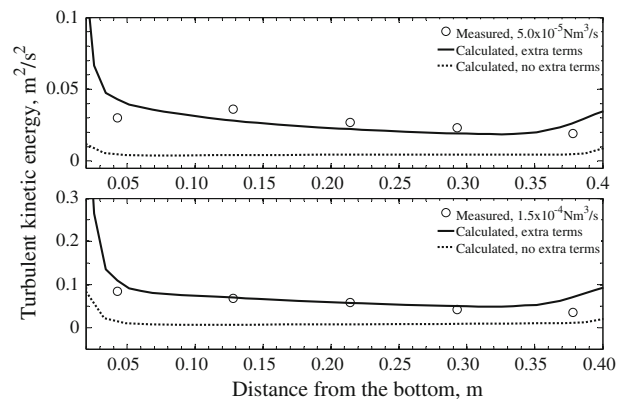

Fig. 5—Comparisons between measured[5,6] and calculated TKE along the center line with gas flow rate $Q = 5.0 \times 10^{-5}$ Nm³/s (upper panel) and $Q = 1.5 \times 10^{-4}$ Nm³/s (lower panel).

TKE dissipation is high and the average bubble contact time (calculated by Eq. [6c]) is insufficient to affect the mass transfer process. In this case, the average TKE dissipation is higher than 0.06 m²/s³, which exceeds the threshold (0.04 m²/s³) suggested by the Alves *et al.*[15] The eddy-cell expression is therefore utilized to compute the mass transfer coefficient of hydrogen in the following sections.

IV. RESULTS AND DISCUSSION

To study the effect of vacuum pressure on hydrogen removal, three cases with different vacuum pressures (P_v) are simulated: 1 mbar for Case 1; 2 mbar for Case 2; and 10 mbar for Case 3. Case 1 corresponds to one of the practical operation conditions in the plant. The initial [H] and Q are given 6.1 ppm and 0.05 Nm³/min, respectively, for the three cases. The hydrogen transport equations are solved based on the stationary flow field obtained with the fluid dynamic model. Some detailed results are shown in Figure 7.

Figure 7(a) shows the transient distribution of hydrogen in the liquid steel bath. As can be seen, [H] decreases during the process and a low [H] zone appears in the gas
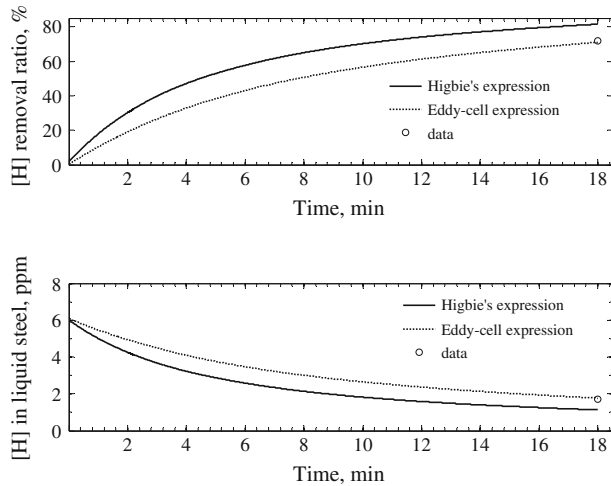

Fig. 6—Evolution of hydrogen removal ratio (upper panel) and hydrogen content in liquid steel (lower panel) with different expressions of mass transfer coefficient.

plume and bath surface. This can be explained by the locally low hydrogen partial pressure in the bubbles and at the surface. It can be also seen that [H] is higher at the place where the circulating flow is high (cf. Figure 7(b)).

In principle, the hydrogen removal could take place through the bubble surface and bath surface. These two routes are compared in Figure 8, where the evolutions of dehydrogenation rate by gas bubbles and bath surface are plotted. The point to be noticed is that the dehydrogenation by the bath surface is actually computed within the grid cells adjacent to the surface. It can be seen that the bubble surface is the main area for hydrogen removal especially at the beginning of the dehydrogenation process. This is because the gas–liquid interfacial area is much higher than that at the bath surface. The dehydrogenation rates for both routes decrease during the process due to the descent of [H] in the liquid bath, which leads to the decay of the driving force for mass transfer, i.e., concentration gradient. However, the dehydrogenation rate at the bath surface does not decrease as much as the one for gas bubbles. This could also be explained by the driving force: The hydrogen content around the open-eye is always in a low level compared to the one in the bulk flow (cf. Figure 7),
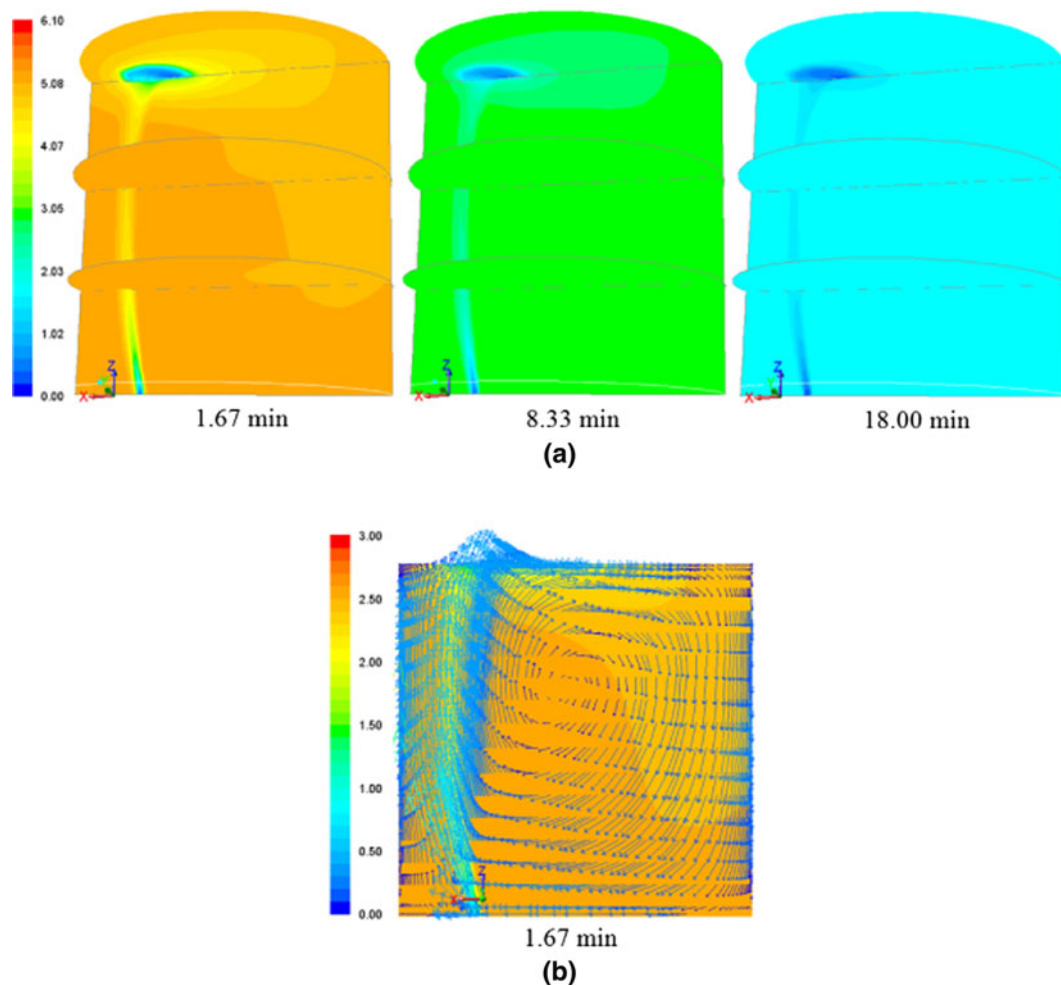

(a)

1.67 min

(b)

Fig. 7—(a) Transient distribution of [H] in the steel bath ([H] in ppm). (b) Hydrogen content with corresponding velocity field (velocity in m/s) for Case 1.
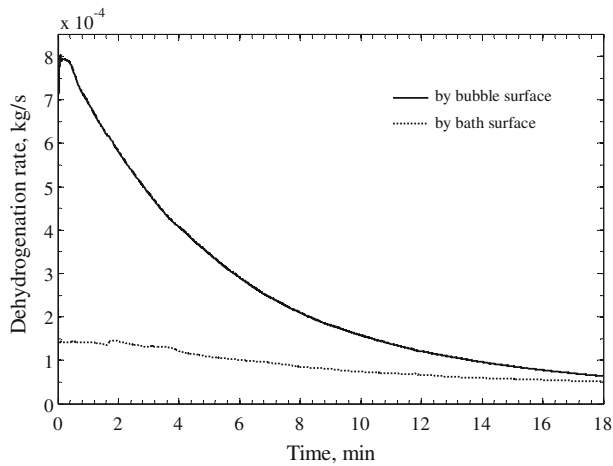
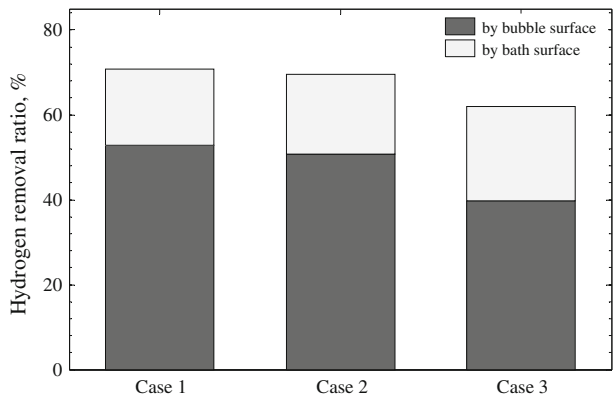Fig. 8—Dehydrogenation rates by gas bubbles and bath surface for Case 1.

Fig. 9—Effect of vacuum pressure on hydrogen removal ratio for Cases 1 to 3.

Fig. 10—Evolutions of hydrogen content in liquid steel for Cases 1 to 3.

Table IV. Operating Condition for Case 4 to 6

	Case 4	Case 5	Case 6
Vacuum pressure (mbar)	0.72	0.78	0.58
Gas flow rate (Nm^3/min)	0.07	0.08	0.1
Calculated period (min)	21	15	20
Initial [H] (ppm)	5.9	5.6	5.8
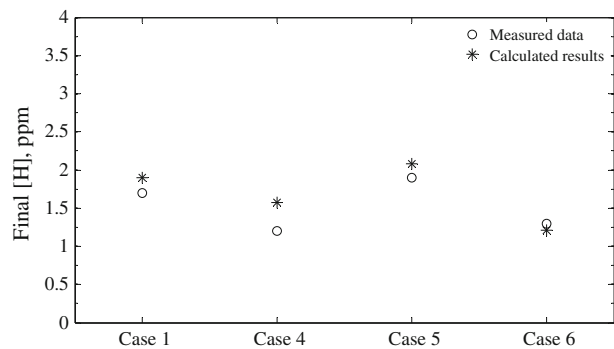
Fig. 11—Comparisons between measured and calculated final [H] for different cases.

giving rise to a lower driving force for the removal reaction at the bath surface. The effect of vacuum pressure on dehydrogenation is illustrated in Figure 9, where the [H] removal ratio for each route, *i.e.*, bubble surface or bath surface, is depicted. It can be seen that the total removal ratio decreases when the vacuum pressure increases since the thermodynamic conditions for dehydrogenation in the liquid bath deteriorate when increasing the vacuum pressure. Furthermore, as shown in the figure, the removal ratio from the bath surface slightly increases for Case 3 with much higher vacuum pressure. This can be explained as follows: The liquid steel with higher [H] (because of worse dehydrogenation conditions in the liquid bath) could reach the bath surface where the partial pressure of hydrogen is fixed due to the assumption of zero-H_2 partial pressure. The driving force of dehydrogenation near the bath surface therefore rises, causing a higher removal ratio at the bath surface.

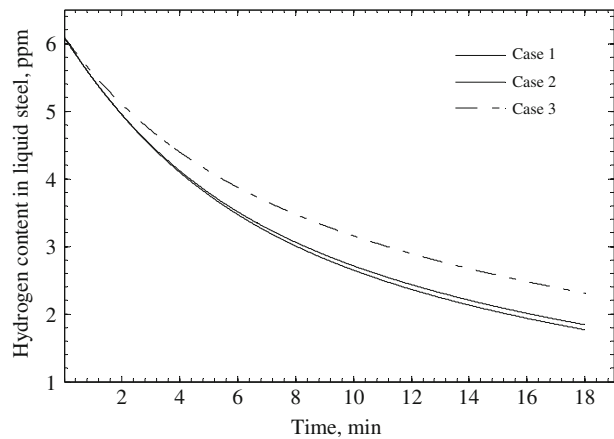The evolutions of [H] under different vacuum pressures are plotted in Figure 10, which reveals that lower [H] could be achieved by reducing the operation pressure. However, the effect of reducing pressure from 2 to 1 mbar is not obvious because the curves of Case 2 and Case 1 displayed in Figure 10 are quite close to each other. This finding is consistent with that reported by Bannenberg et al.[2]

In order to further validate the integrated numerical model, three more cases corresponding to practical conditions in Riva Caronno Works are performed. The operating conditions for Case 4 to 6 are listed in Table IV. The calculated final [H] for Case 4 to 6 as well as that of Case 1 is plotted in Figure 11, where the measured data from the plant are also plotted. As can be seen, the biggest deviation of 6.2 pct occurs with Case 4; a good agreement is still achieved between prediction and measurement.

V. CONCLUSIONS AND FUTURE WORK

A comprehensive numerical model has been developed to simulate the fluid flow and dehydrogenation of liquid steel in an industrial vacuum degasser. Mass and momentum equations based on the Euler–Euler method were solved and the extended k–ε turbulence equations were adopted to consider the effect of gas injection on the turbulent properties. The fluid dynamic sub-model was verified with a physical water model (from literature), which is believed to have similar flow phenomena as the current studied vacuum degasser on the basis of the modified Froude number. For solving the species transport equations of hydrogen, an IAC model was introduced to compute the bubble–liquid interfacial area density, and moreover both Higbie's and eddy-cell expressions were evaluated to obtain proper hydrogen mass transfer coefficient for the system. The results showed that

– The extended k–ε turbulence model is more accurate than the standard k–ε model to simulate the gas-steel flow phenomena in the vacuum degassers.
– Eddy-cell expression for mass transfer coefficient gives better agreement with the plant data compared with Higbie's expression. However, it must be noted that only one case was modeled. This statement is also supported by Alves et al.,[15] who pointed out that Higbie's expression could be more suitable for the system with a low level of TKE dissipation.
– Hydrogen removal takes place at the bubble surface and bath surface. The bubble surface is the main area for hydrogen removal especially at the beginning of dehydrogenation.
– Lower [H] could be achieved by reducing the operation pressure in a vacuum degasser. The calculations showed the following results: 2.3 ppm for 10 mbar, 1.84 ppm for 2 mbar, and 1.77 ppm for 1 mbar. Only the vacuum pressure was changed in these three calculations.
– The developed model is accurate enough to predict the dehydrogenation process in the industrial vacuum tank degasser. As depicted in Figure 11, the model predictions showed good agreement with the measured data from Riva Caronno Works. This implies that the simplifications and assumptions made in the model are appropriate.

In the future, the integrated model will be further developed. The hydrogen source in lime will be considered and the effect of carbon, oxygen in liquid steel on hydrogen removal will be investigated since the formation of CO bubbles under vacuum treatment could provide a third reaction site for dehydrogenation. Also, the model will be applied to the effect of different blowing methods, e.g., single bottom blowing or double bottom blowing.

LIST OF SYMBOLS

VARIABLES

A	Area (m^2)
a	Interfacial area concentration (m^2/m^3)
C_L, C_D	Coefficients (–)
$C_{1\varepsilon}$, $C_{2\varepsilon}$, C_{k1}, C_{k2}, $C_{\varepsilon 1}$, $C_{\varepsilon 2}$	Constants for turbulent model (–)
C_f	Friction factor (–)
D	Mass diffusion coefficient (m^2/s)
d	Diameter (m)
F	Lift force (N/m^3)
f	$(1 - \alpha_p)^{1.5}$ (–)
G	Production term (kg/m s^3)
g	Acceleration of gravity (m/s^2)
H	Liquid bath height (m)
h	Height of cells above the bubble (m)
J	Diffusion flux (kg/m^2 s)
K	The equilibrium constant (ppm/Pa$^{1/2}$)
k	Turbulent kinetic energy (m^2/s^2)
L	Laplace length (m)
P	Pressure (Pa)
Q	Volume flow rate (Nm^3/s)
R	Drag force (N/m^3)
r	Radius (m)
Re	Reynolds number (–)
S	Source term (for k: kg/m s^3; for ε: kg/m s^4; for species transport: kg/m^3 s; for IAC: m^{-1} s^{-1})
T	Temperature (K)
u	Velocity (m/s)
V	Volume (m^3)
w	Velocity (m/s)
Y	Mass fraction (–)

GREEK

α	Volume fraction (–)
ε	Turbulent dissipation ratio (m^2/s^3)
θ	Bubble relaxation time (seconds)

κ	Mass transfer coefficient (m/s)
λ_{RT}	Rayleigh–Taylor instability wavelength (m)
μ	Dynamic viscosity (kg/m s)
v	Kinematic viscosity (m^2/s)
ξ	Activity coefficient(–)
π	Constant (–)
τ	The residence time of liquid (seconds)
ρ	Density (kg/m^3)
σ	Constant (–)
φ	Variable index
ψ	Interaction coefficient (–)

WE	Wake-entrainment
ε	Turbulent dissipation

ACCENT

~	Non-dimensional

SUBSCRIPTS

0	Initial
b	Bubble
cap	Strongly deformed regime
cv	Control volume
dis	Distorted bubble regime
e	Equilibrium
eff	Effective
fs	Free surface
g	Gas
H	Hydrogen
H$_2$	Hydrogen gas
hyc	Hydraulic
i	Species: [H] or H$_2$
ii	Cells above the bubble
j	Element in liquid steel
k	Turbulent kinetic energy
l	Liquid
mole	Molecular
m	Mixture
md	Modified
p	Phase index
pq	Interaction between phase p and phase q
q	Phase index
RC	Random collision
r	Radial direction
slip	Relative velocity
TI	Turbulent impact
t	Turbulence
v	Vacuum
vis	Viscous regime

REFERENCES

1. R. Dekkers, B. Blanpain, J. Plessers, and P. Wollants: *VII International Conference on Molten Slags Fluxes and Salts*, The South African Institute of Mining and Metallurgy, Johannesburg-South Africa, 2004, p. 753.
2. N. Bannenberg, B. Bergmann, and H. Gaye: *Steel Res.*, 1992, vol. 63 (10), pp. 431–37.
3. J.F. Domgin, P. Gardin, and M. Brunet: *2nd International Conference on CFD in the Minerals and Process Industries*, CSIRO, Melbourne, Australia, December 1999, p. 181.
4. M.P. Schwarz: *Appl. Math. Model.*, 1996, vol. 20, pp. 41–51.
5. Y.Y. Sheng and G.A. Irons: *Metall. Trans. B*, 1993, vol. 24B, pp. 695–705.
6. Y.Y. Sheng and G.A. Irons: *Metall. Trans. B*, 1992, vol. 23B, pp. 779–88.
7. J.L. Xia, T. Ahokainen, and L. Holappa: *Scand. J. Metall.*, 2001, vol. 30, pp. 69–76.
8. F.J. Moraga, D.A. Drew, and R.T. Lahey, Jr.: *J. Fluids Eng.*, 2004, vol. 126, pp. 573–77.
9. A. Jauhiainen, L. Jonsson, P. Jönsson, and S. Eriksson: *Steel Res.*, 2002, vol. 73 (3), pp. 82–90.
10. M. Hallberg, L. Jonsson, and J. Alexis: *SCANMET I*, MEFOS, Luleå-Sweden, 1999, p. 119.
11. D. Mazumdar and J.W. Evans: *Modeling of Steelmaking Processes*, 1st ed., CRC Press, Boca Raton, 2010, p. 18.
12. P.G. Jönsson and L.T.I. Jonsson: *ISIJ Int.*, 2001, vol. 41 (11), pp. 1289–1302.
13. A.M. Celiberto, P.C. Fernandes, and J.L. Boschetti: *16th Steelmaking Conference*, Instituto Argentino de Siderurgia, Rosario-Argentina, November 2007.
14. R. Higbie: *Trans. AIChE*, 1935, vol. 31, pp. 365–89.
15. S.S. Alves, J.M.T. Vasconcelos, and S.P. Orvalho: *Chem. Eng. Sci.*, 2006, vol. 61, pp. 1334–37.
16. S. Taniguchi, S. Kawaguchi, and A. Kikuchi: *2nd International Conference on CFD in the Minerals and Process Industries*, CSIRO, Melbourne-Australia, December 1999, p. 193.
17. *ANSYS FLUENT 14.0 Theory Guide*, 2011, Ansys Inc.
18. *ANSYS FLUENT 14.0 UDF Manual*, 2011, Ansys Inc.
19. R.P. Stone, D.A. Vensel, and E.T. Turkdogan: *Steelmaking Conference Proceedings*, vol. 74, Washington, D.C., U.S.A., April 1991, p. 761.
20. S. Misra, Y. Li, and I.I. Sohn: *Iron Steel Technol.*, November 2009, pp. 43–52.
21. Q. Wu, S. Kim, and M. Ishii: *Int. J. Heat Mass Transf.*, 1998, vol. 41, pp. 1103–12.
22. T. Hibiki and M. Ishii: *Int. J. Heat Mass Transf.*, 2002, vol. 45, pp. 2351–72.